nature astronomy
SUPPLEMENTARY INFORMATION
VOLUME: 1 | ARTICLE NUMBER: 0004
In the format provided by the authors and unedited.

Variability in the atmosphere of the hot giant planet HAT-P-7 b

Tables

Parameter	Unit	Value
System		
KIC	-	10666592
P	d	2.2047354±0.0000001
T_0	BJD†-2454833	121.358572±0.000004
a/R_*	-	$4.1545^{+0.0029}_{-0.0025}$
i	degrees	$83.143^{+0.023}_{-0.020}$
Star		
T_*	K	6350±80
R_*	R_{sun}	$1.84^{+0.23}_{-0.11}$
M_*	M_{sun}	$1.47^{+0.08}_{-0.05}$
u_1	-	$0.3497^{+0.0026}_{-0.0035}$
u_2	-	$0.1741^{+0.0057}_{-0.0044}$
Planet		
R_p	R_J	$1.419^{+0.178}_{-0.085}$
R_p/R_*	-	$0.077524^{+0.000017}_{-0.000022}$
M_p	M_J	1.63±0.13
A_3	ppm	-1.93±0.23
Θ_3	phase	$0.0163^{+0.0054}_{-0.0052}$
Doppler/Ellipsoidal		
α_1	-	0.0657
α_2	-	1.22
α_d	-	3.41

Table 1: HAT-P-7 Input Parameters[6]. † BJD=Barycentric Julian Date.

Figures

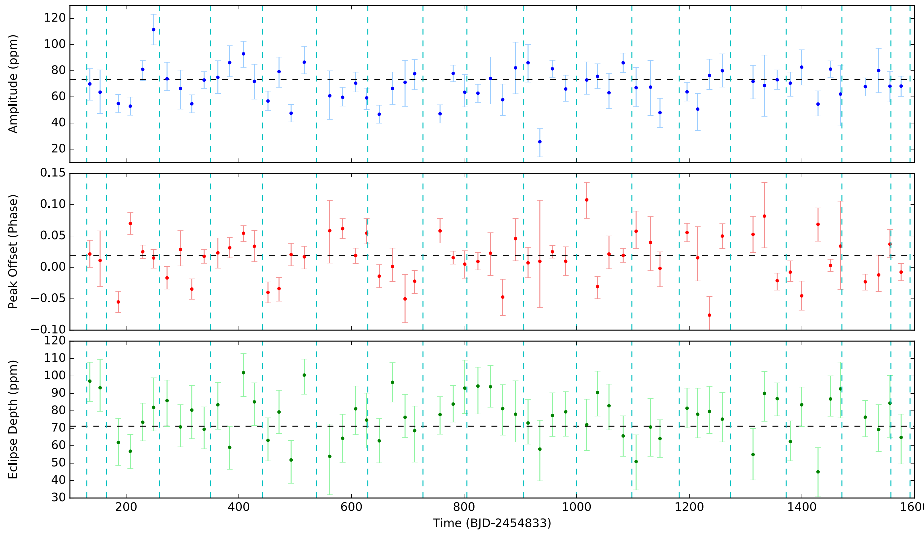

Supplementary Figure 1: Independent best fitting parameters. Variation in peak amplitude (top, blue), peak offset (middle, red) and secondary eclipse depth (bottom, green). Best fit parameters resulting from fits to discrete lightcurve segments are shown, resulting in fewer, but independent, points than the convolution method leading to Figure 1. The Kepler quarter boundaries are shown as vertical dashed lines. Error bars are 1σ errors on the fit parameters.

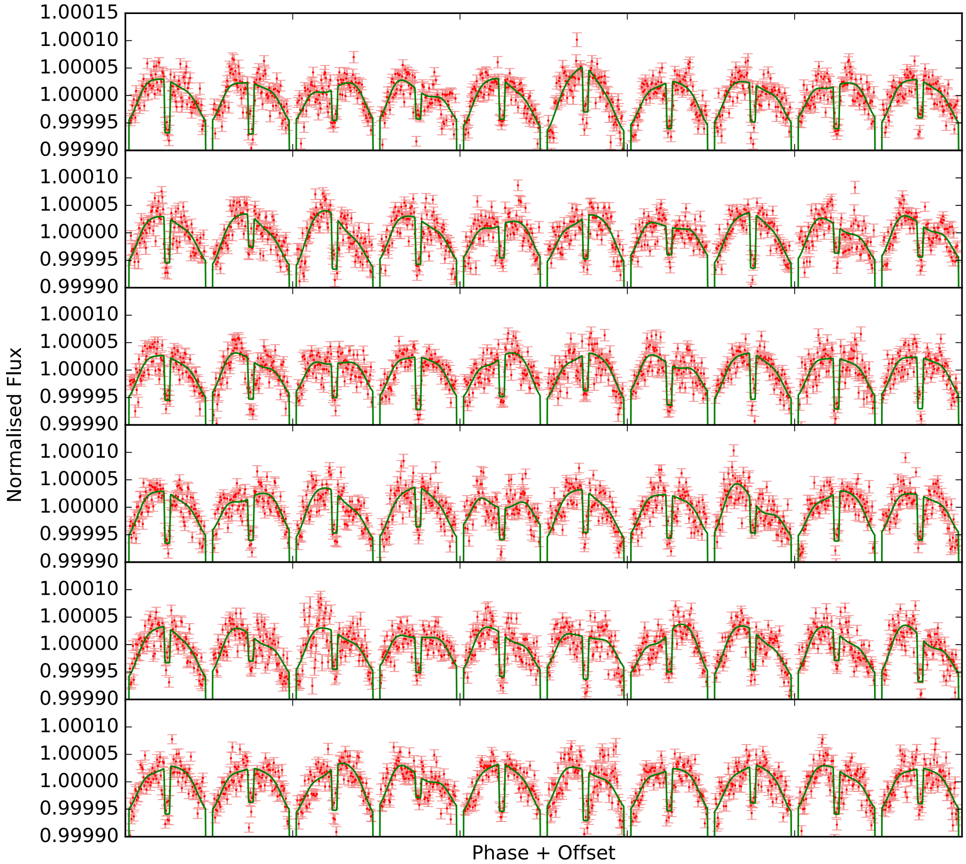

Supplementary Figure 2: The data segments used to derive the fit parameters of Supplementary Figure 1. The best fit models are plotted in green. Reading left to right and top to bottom, they correspond to each datapoint shown in that Figure. Each segment has been binned to 100 bins for clarity. Error bars are the standard error on the mean of the datapoints contributing to each bin.

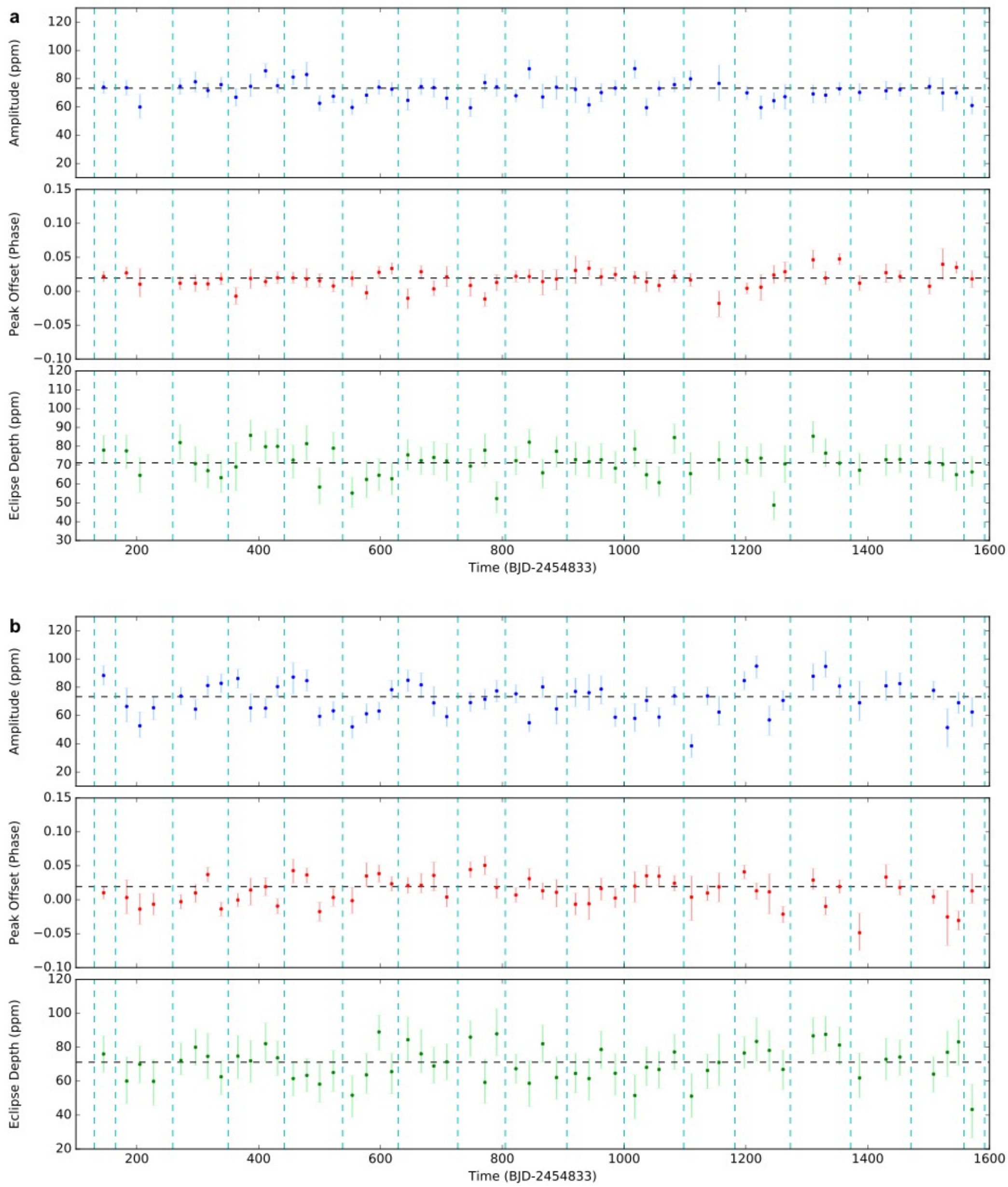

Supplementary Figure 3: Best fitting parameters from injection tests. Panel a: As Supplementary Figure 1 for KIC11027406 after injection with a constant HAT-P-7 b phase curve. Panel b: As Supplementary Figure 1, for KIC10861893 after injection with a constant HAT-P-7 b phase curve. Marginally significant variation in A_p is seen for KIC10861893, implying the presence of systematic noise biasing the fits. The variations in Θ, while showing some structure, are on a much smaller scale than those observed in HAT-P-7 b. Error bars are 1σ errors on the fit parameters.

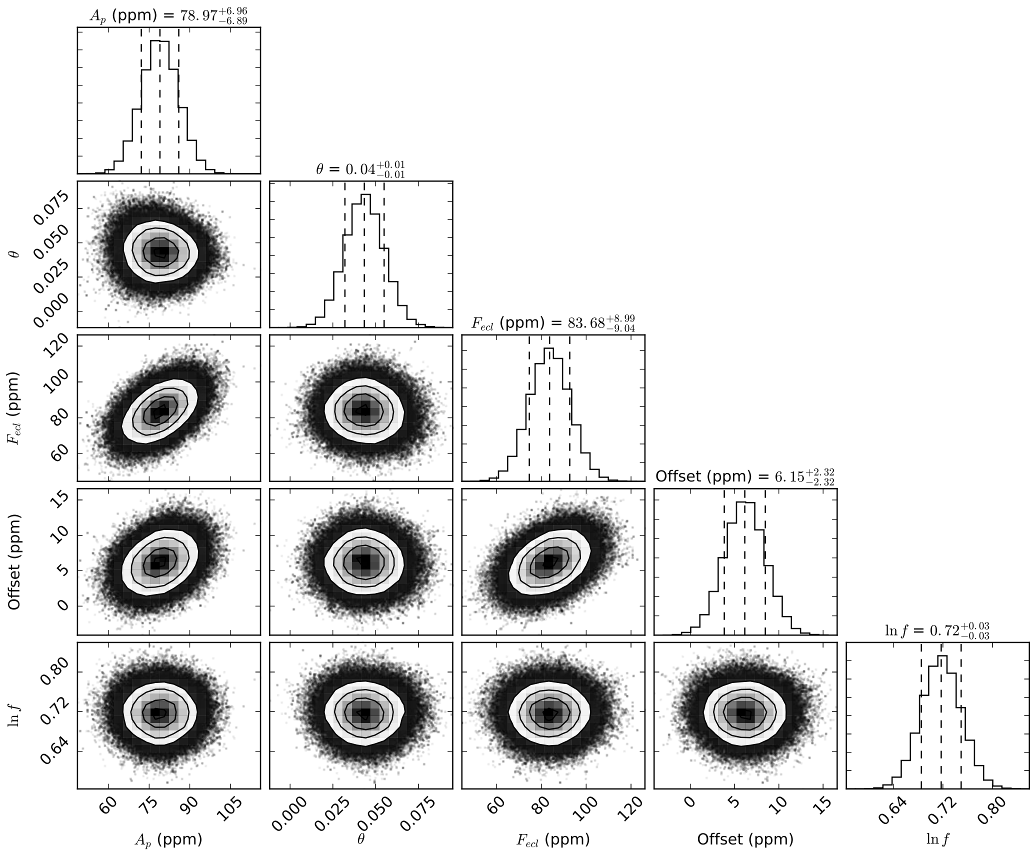

Supplementary Figure 4: MCMC parameter correlations. Triangle plot of an MCMC run applied to a phase curve segment at time 226 (BJD-2454833), with significant positive Θ. The outputs are consistent with those of the prayer bead analysis, although the errors from the MCMC are slightly smaller. The larger errors are used for final values. An additional parameter, f, is fit for which scales up the errors by a factor of ~2, to account for correlated noise not present in the given errors.

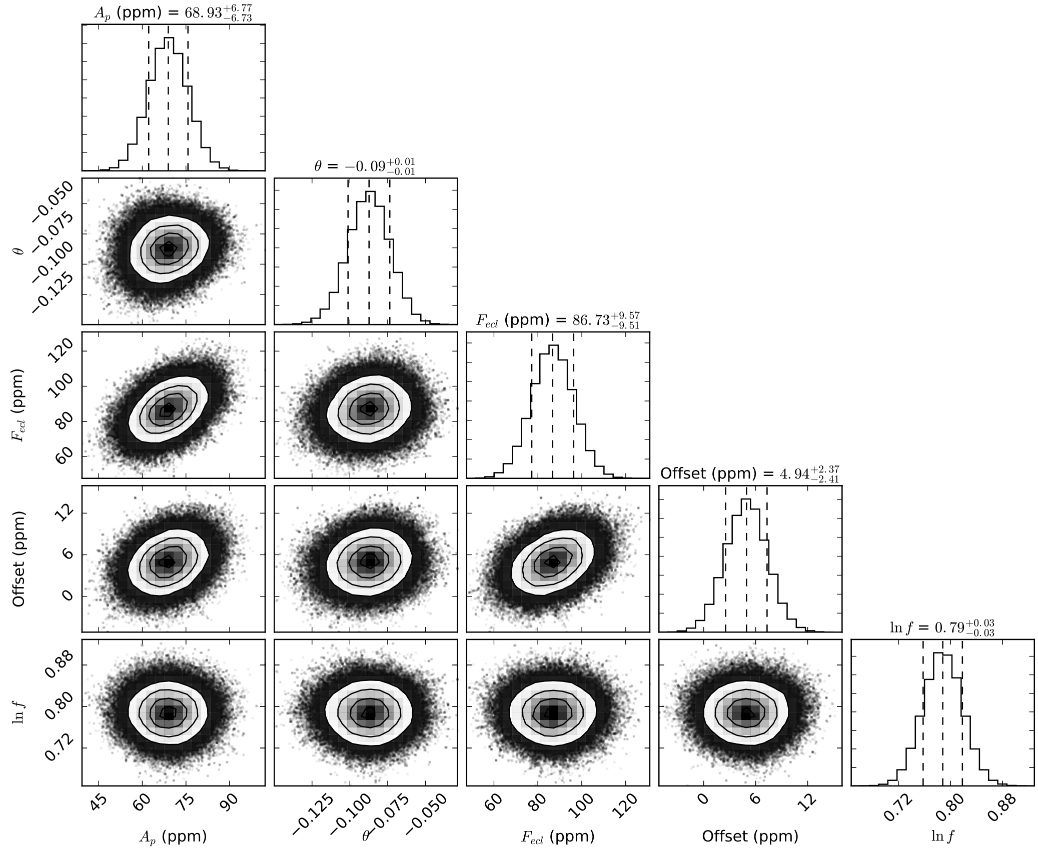

Supplementary Figure 5: MCMC parameter correlations. As Supplementary Figure 4 for a phase curve segment at time 1238 (BJD-2454833). This segment has significant negative Θ. The parameters are again consistent with the prayer bead results, with the MCMC analysis giving slightly smaller errors.

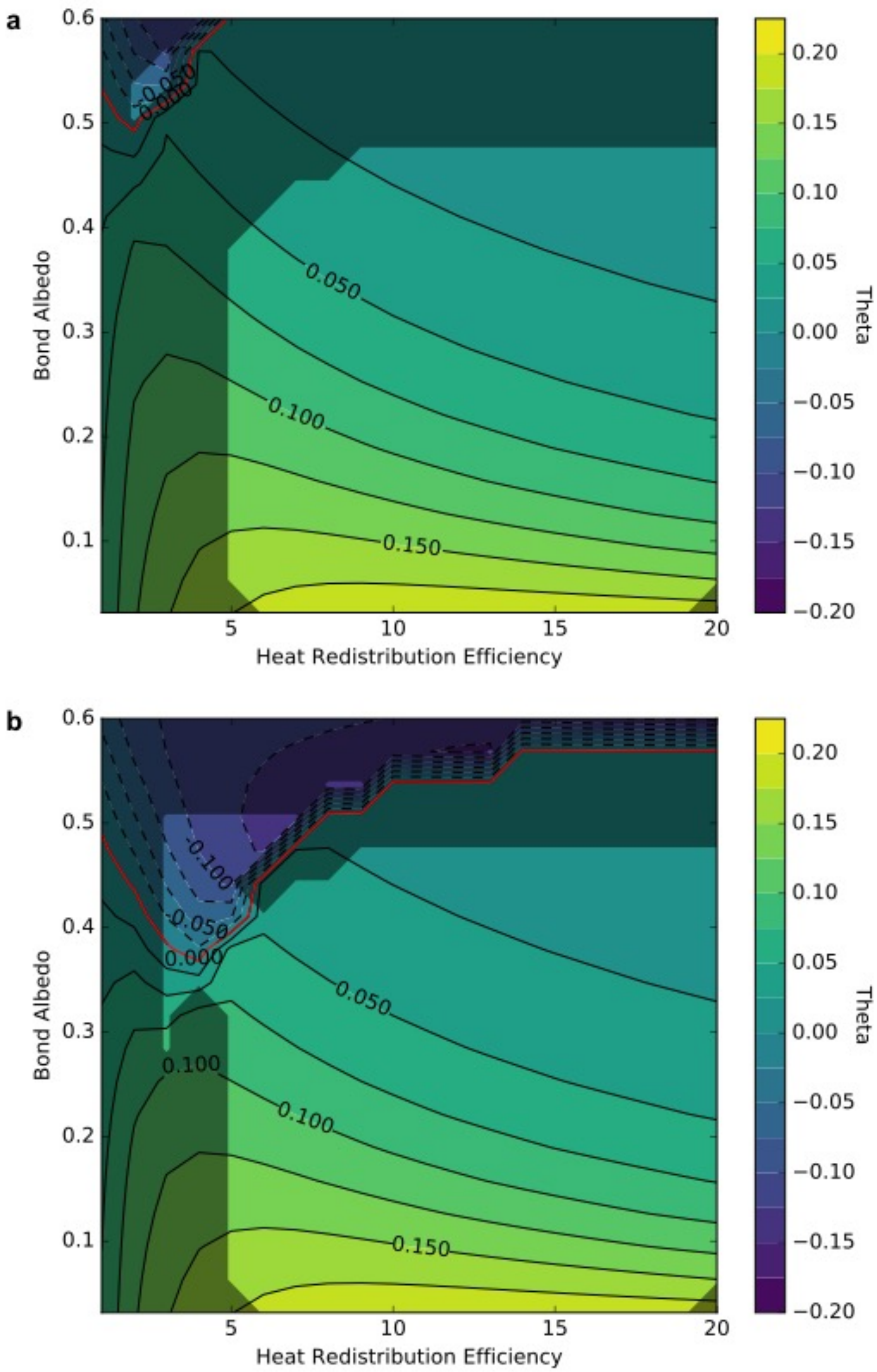

Supplementary Figure 6: Peak offset predicted by model. As Figure 4 for $T_C = 1600K$ (top), $T_C = 1800K$ (bottom) and κ=40. Reducing the value of κ makes negative contours less deep, but does not change the structure of the grid. Producing all the observed values of Θ requires transitioning through a regime disallowed by the observed amplitude, but is possible.

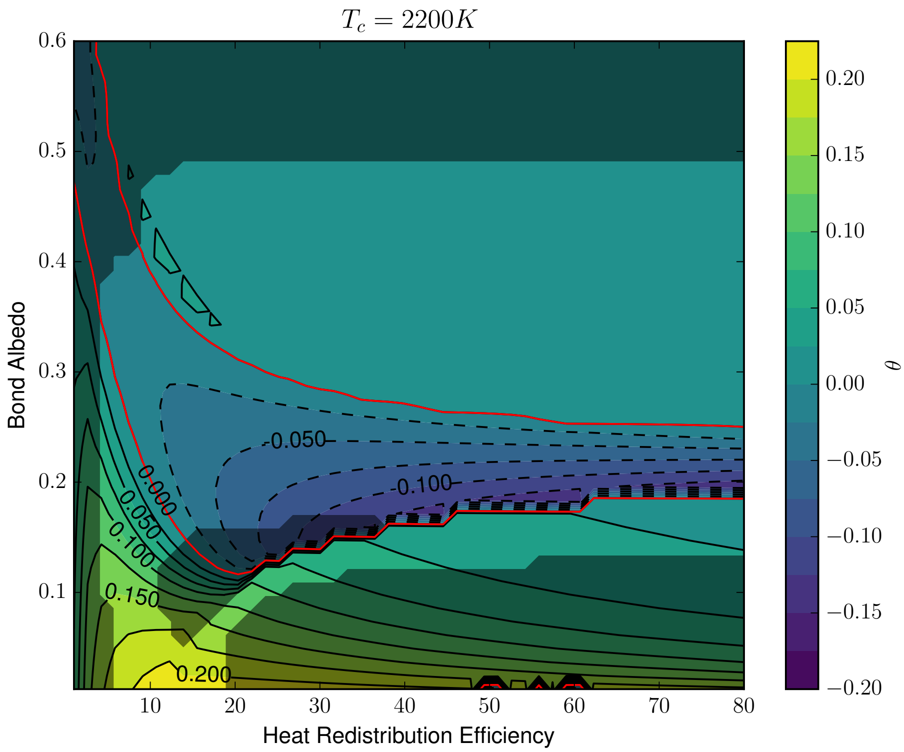

Supplementary Figure 7: Peak offset predicted by model. As Figure 4 for T_C = 2200K and κ=40. Reducing the value of κ makes negative contours less deep, but does not change the structure of the grid. The grid has been extended up to ε=80, as it is not possible to achieve the maximum negative offset in the previously used ε=[0,20] grid range.

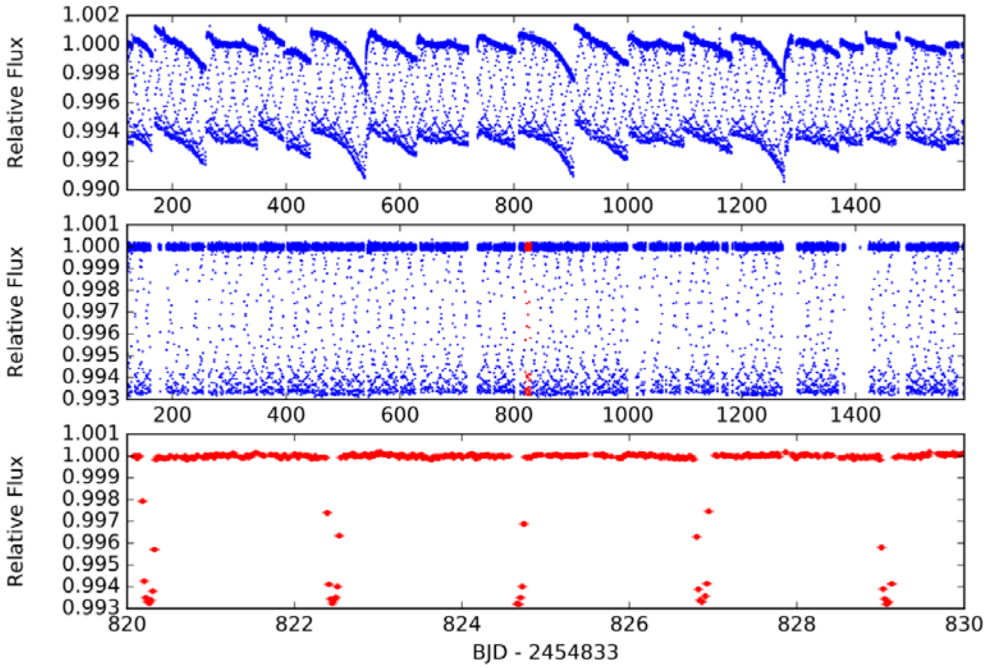

Supplementary Figure 8: Lightcurve detrending process. Kepler data of HAT-P-7 before detrending (top), after detrending (middle) and zoomed in to show 4 planetary orbits (bottom).

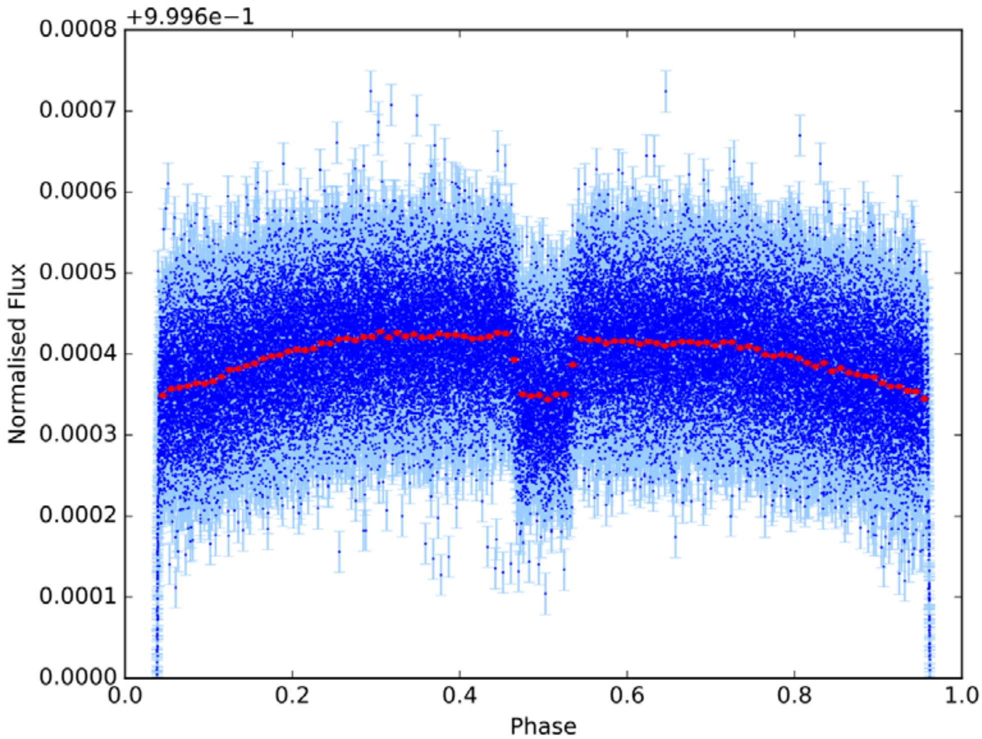

Supplementary Figure 9: HAT-P-7 b phase curve, showing the entire dataset. The unbinned data are in blue, and 100 bins shown in red. The planetary transit is at phase 0 and is below the scale of the graph. Error bars are the 1σ photometric errors on each datapoint.

Phase curve model

We use the model of [6]. This is summarised here for clarity. As HAT-P-7 b has no detectable eccentricity [9,10], we assume circular orbits throughout.

The model is comprised of five components: a quadratically limb darkened Mandel-Agol transit model F_{transit} [41], using the parameters given in Supplementary Table 1 (although note that datapoints in transit were removed before fitting), contributions from the planetary mass F_m, the secondary eclipse F_{ecl}, the planetary brightness F_p, a cosine third harmonic of the planet's period F_3, and an offset C. The combined flux at phase ϕ is given by

$$F(\phi) = F_{\mathrm{transit}}(\phi)F_m + F_{\mathrm{ecl}}(\phi) + F_p(\phi + \theta) + F_3(\phi - \theta_3) + C$$

with

$$\phi = 2\pi \frac{t - T_0}{P}$$

where T_0 represents the first mid-eclipse time, and P the planetary orbital period.

The planetary brightness F_p is defined by a Lambert sphere, with

$$F_p = A_p \frac{\sin z + (\pi - z)\cos z}{\pi}$$
$$\cos z = -\sin i \cos(2\pi(\phi + \theta))$$

where A_p is the peak amplitude, θ is the phase offset in peak brightness, and i is the planetary orbital inclination.

The secondary eclipse is modelled as a second Mandel-Agol transit, for the occultation of a uniform source with the planetary parameters given in Supplementary Table 1, with depth F_{ecl}. F_{ecl} and the above F_p component are allowed to vary as a function of time, and are refit for each subsection of the lightcurve considered.

The planetary mass contributes through both Doppler boosting and ellipsoidal variation. Doppler boosting arises from the changing radial velocity of the host star as the planet orbits. When the star is moving towards the observer, the stellar flux is increased via Doppler boosting and also blueshifted, resulting in a changing contribution within the *Kepler* bandpass. The reverse occurs when the star moves away from the observer. Ellipsoidal variation results due to changes in the visible surface area of the star. The stellar surface has a tidal bulge associated with the planet – as the planet orbits, this bulge moves into and out of visibility, changing the visible flux. The planetary mass contribution is given by

$$F_m = M_p \left\{ \left(\frac{2\pi G}{P}\right)^{1/3} \frac{\alpha_d \sin i}{c M_*^{2/3}} f_d - \frac{\alpha_2 \sin^2 i}{M_*} f_e \right\}$$

where M_p is the planet's mass, G the gravitational constant, M_* the stellar mass, c the speed of light, and α_d the photon-weighted bandpass-integrated beaming factor. The values of α_d and α_2

are given in Supplementary Table 1, and are taken from [6]. f_d and f_e are the phase dependent components of the Doppler boosting and Ellipsoidal signals respectively. They are given by

$$f_d = \sin(2\pi\phi)$$
$$f_e = \left(\frac{a}{R_*}\right)^{-3} \cos(4\pi\phi) + \left(\frac{a}{R_*}\right)^{-4} f_1 \cos(2\pi\phi) + \left(\frac{a}{R_*}\right)^{-4} f_2 \cos(6\pi\phi)$$

with f_1 and f_2 determine the amplitude of higher order ellipsoidal variations, and are given by

$$f_1 = 3\alpha_1 \frac{5\sin^2 i - 4}{\sin i}$$

$$f_2 = 5\alpha_1 \sin i$$

The value for α_1 is given in Supplementary Table 1, and is as calculated in [6].

Lastly, the cosine third harmonic is described by

$$F_3 = A_3 \cos\big(6\pi(\phi - \theta_3)\big)$$

with A_3 the third harmonic amplitude and θ_3 the phase offset of the signal. This third harmonic signal was discovered in [6], and has an unknown origin. We include it with their parameters, and hold it constant with time.

Of all the parameters mentioned here, most are held constant at their values fit from the whole dataset. The parameters allowed to vary between lightcurve segments are A_p, θ, F_{ecl}, and C, the latter to allow for small shifts in flux between segments. We hold the remaining parameters constant to simplify the model, and because their effect is expected to be negligible on the phase curve itself. We discuss those parameters which could impact the phase curve here:

Orbital Period: The published value and error used[6] lead to an error of less than one *Kepler* cadence in phasing over the entire dataset, and less over each phase curve chunk. Hence we consider the effect negligible.

Epoch: As above with the orbital period, the published value and error lead to an effect of less than one *Kepler* cadence.

Planet Mass: See Methods for a test of the effect of fixing the mass, which led to no significant effect.

Third Harmonic: This harmonic was detected at a level of 2ppm[6], at 8.4σ significance using the entire dataset. We are unable to detect the harmonic in a 10 orbital period phase curve chunk. As such, while the harmonic is included in the model, fitting for it simultaneously would have negligible effect.

Radii Ratio: The primary transit is removed before fitting. However, the planet to star radius ratio affects the shape of ingress and egress of the secondary eclipse. Given the constraints found on secondary eclipse depth variation (51% at 3σ), the shape of ingress or egress of the secondary eclipse is not well determined enough to have any significant effect.

Supplementary Information References

41. Mandel, K. & Agol, E. Analytic light curves for planetary transit searches. *Astrophys. J.* **580,** L171–L175 (2002)

Other Files

Video 1: Visualisation of the dayside of HAT-P-7b. See Methods for description, and for the assumptions used to simulate the dayside emission.

Dataset 1: fitparams_table.csv (51kb): Values for individual fits and their errors. Columns are described in the file header.